Published online May 6, 2005

Scaling of Infiltration and Redistribution of Water across Soil Textural Classes

Joseph A. Kozak* and Lajpat R. Ahuja

ABSTRACT

Results with an empirically based one-parameter model showed that the pore-size distribution index (λ) described in the Brooks and Corey formulation of soil hydraulic properties can scale the soil–water retention curves below the air-entry pressure head (ψ_b) values across dissimilar soils. It is shown here that ψ_b and saturated hydraulic conductivity (K_s) are also strongly related to λ, and thus all hydraulic parameters may be estimated from λ. The major objective here was to examine how these relationships to λ lead to relationships for infiltration and soil water contents during redistribution across soil textural classes. The Root Zone Water Quality Model simulated infiltration for four rainfall intensities and two initial pressure head conditions and redistribution for four initial wetting depths and two initial pressure head conditions in 11 textural class mean soils. All infiltration results across textural classes were scaled quite well by using the λ-derived normalization variables based on the dimensional analysis of the Green–Ampt model. Thus, if infiltration for one soil (λ) is known, infiltration for other soils (λs) can be estimated. Additionally, we present infiltration, as well as redistribution, as explicit functions of λ. These functions can be used to approximately estimate infiltration and soil water contents across soil types for other soils and conditions by interpolation. This study enhances our understanding of the soil–water relationships among soil textural classes, and hopefully, provides a basis of further studies under field conditions for (i) estimating spatial variability of soil water for site-specific management and (ii) for scaling up results in modeling from plots to fields to watersheds.

Scaling has been used as a tool for approximately describing field spatial variability of soil hydraulic properties, specifically the matric potential and unsaturated hydraulic conductivity as a function of soil water content (e.g., Warrick et al., 1977; Simmons et al., 1979; Russo and Bresler, 1980) as well as characteristics derived from these, such as infiltration (Sharma et al., 1980). The frequency distribution and spatial–correlation structure of scaling factors describe variability in the field, thus resulting in considerable simplicity and enhanced understanding as well as convenience in modeling a heterogeneous watershed for its hydrologic responses (Pachepsky et al., 2003; Nielsen et al., 1998; Peck et al., 1977; Sharma and Luxmoore, 1979; Warrick and Amoozegar-Fard, 1979; Ahuja et al., 1984). Inversely, scaling can also be used to estimate soil hydraulic properties at different locations in a watershed from measurement of these properties at one representative location and limited data at other locations (Ahuja et al., 1985; Williams and Ahuja, 1991).

Two methods to derive the scaling factors are well-known (Tillotson and Nielsen, 1984): (1) the dimensional analysis technique, which is based on the existence of physical similarity in the system; and (2) the empirical method, called functional normalization, which is based on regression analysis. The similar-media scaling of Miller and Miller (1956) and the fractal-based approaches of Tyler and Wheatcraft (1990), Rieu and Sposito (1991), and Hunt and Gee (2002a, 2002b) are examples of the first method. Most of the scaling work cited above has extended the similar-media scaling concept to field soils that are generally "non-similar" by invoking additional empirical assumptions and using a regression method.

Very limited research has been done on relating soil hydraulic properties across widely dissimilar soil textural classes. Gregson et al. (1987) showed that the slope and intercept of the commonly used Brooks and Corey (1964) log–log relationship for soil matric potential versus water content, below the air-entry value, was highly correlated across 41 Australian and British soil classes. This formed the basis for their one-parameter model for estimating the soil water retention curve in any soil. In a recent book chapter, Williams and Ahuja (2003) showed that: (1) there was a strong relationship between the intercepts and slopes of textural class mean water retention curves (obtained using the geometric mean Brooks–Corey parameters) for 11 U.S. soil classes from sand to clay (Rawls et al., 1982); and (2) these curves could be scaled very well (brought together closely) using their slopes as scaling factors. As a part of this study we found that K_s and the air-entry or bubbling pressures of these textural class mean curves also had a strong logarithmic relation with their slopes. The air-entry value on the log–log water retention curve defined by the slope–intercept relation also determines the saturated soil water content.

Further, if we accept the assumption that the unsaturated hydraulic conductivity curve can be estimated from the known water retention curve, and K_s value, as established by numerous investigations (See Green et al., 1982; Campbell, 1974) and used commonly by modelers, the slope of the log–log water retention curve, λ, can be used to estimate the conductivity curve as well. Thus, the slope of the water retention curve determines the soil hydraulic properties instrumental in infiltration and soil water redistribution.

The above relationships between λ and soil hydraulic properties were derived through empirical means. Part of these relationships and correlations may be explained through physical–statistical approaches, such as the fractal theory (Tyler and Wheatcraft, 1990; Hunt and Gee, 2002a, 2002b; Rieu and Sposito, 1991). However, real soil systems are more complex, and these approaches have yet to explain the above relationships across soil textural classes. Further research to establish these relations is a challenge for the future.

USDA-ARS, Great Plains Systems Research Unit, 2150 Centre Ave., Building D, Suite 200, Fort Collins, CO 80526. Received 2 Mar. 2004. Soil Physics. *Corresponding author (Joseph.Kozak@npa.ars.usda.gov).

Published in Soil Sci. Soc. Am. J. 69:816–827 (2005).
doi:10.2136/sssaj2004.0085

677 S. Segoe Rd., Madison, WI 53711 USA

Table 1. Hydrological properties of 11 textural classes.

Texture	Mean total porosity, θ_s	Geometric mean bubbling pressure, $\lvert\psi_b\rvert$	Mean residual saturation, θ_r	Geometric mean pore size distribution index	Mean saturated hydraulic conductivity	Intercept *a* from Fig. 1b
	$cm^3\ cm^{-3}$	kPa	$cm^3\ cm^{-3}$	λ	$cm\ h^{-1}$	
Sand	0.437	0.726	0.02	0.591	21.00	−1.79
Loamy sand	0.437	0.869	0.035	0.474	6.11	−2.07
Sandy loam	0.453	1.466	0.041	0.322	2.59	−2.38
Loam	0.463	1.115	0.027	0.22	1.32	−3.67
Silt loam	0.501	2.076	0.015	0.211	0.68	−2.69
Sandy clay loam	0.398	2.808	0.068	0.25	0.43	−3.42
Clay loam	0.464	2.589	0.075	0.194	0.23	−3.91
Silty clay loam	0.471	3.256	0.04	0.151	0.15	−4.39
Sandy clay loam	0.430	2.917	0.109	0.168	0.12	−5.70
Silty clay loam	0.479	3.419	0.056	0.127	0.09	−5.54
Clay	0.475	3.73	0.09	0.131	0.06	−5.98

The objectives of this study were to examine how the above empirical λ-hydraulic properties relations lead to relationships of λ to infiltration and soil water redistribution: (1) to see if λ-based normalizing variables could be used to scale infiltration results across texture classes based on the dimensional analysis of the Green–Ampt model; and (2) to explore any direct explicit relationships among λs and cumulative infiltration as well as redistribution of soil water with time. For these objectives we utilized the Agricultural Research Service's Root

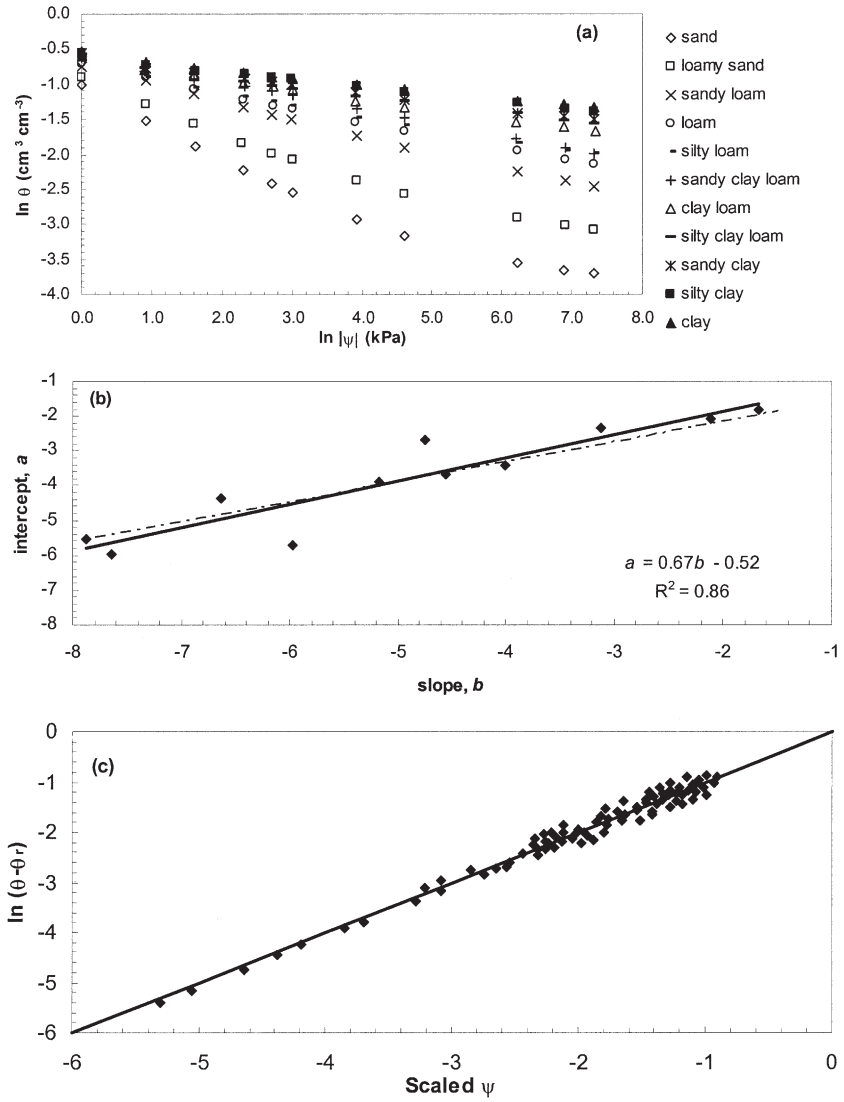

Fig. 1. (a) Soil water characteristic curves calculated for each texture class using Eq. [1] and average hydrologic properties; (b) Relationship of the slope, *b*, and intercept, *a*, (solid line) calculated with Eq. [1] and [2] and the average hydrologic properties for each texture class. Using the *p* and *q* values of Gregson et al. (1987), the slope (dash line) was calculated for each textural class based on Eq. [1] (Williams and Ahuja, 2003); (c) Results of scaling the soil water characteristic for the 11 texture classes (Williams and Ahuja, 2003).

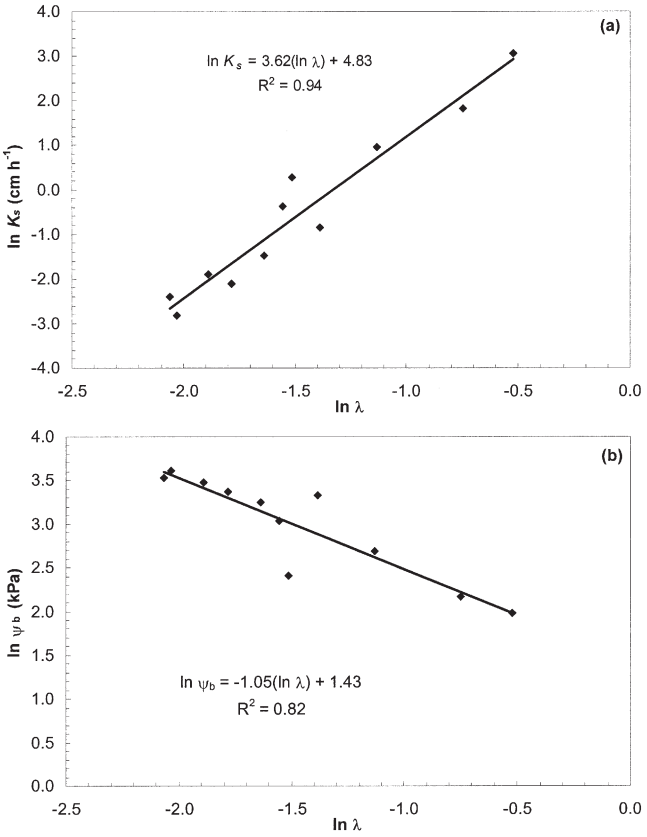

Fig. 2. (a) Log–log relationship between K_s and λ for the 11 textural classes; (b) Log-log relationship between ψ_b and λ for the 11 texture classes.

Zone Water Quality Model (RZWQM) to generate simulated infiltration under four rainfall intensities and redistribution of soil water following four initial wetting depths.

THEORETICAL BACKGROUND AND DEVELOPMENT

Table 1 gives the mean Brooks and Corey (1964) hydrological parameters for water retention and saturated hydraulic conductivity for 11 textural classes from the USA (Rawls et al., 1982). These parameters were based on 1323 soils with approximately 5350 horizons compiled from data of nearly 400 soil scientists. Figure 1a gives an ln-ln[1] graph of the mean curves of different textural classes based on the mean parameter values of Table 1.

[1] Throughout the manuscript, we use ln to denote the natural logarithm to the base e and log to denote the logarithm to the base 10.

A modified form of the soil–water retention curve below the air-entry values is fitted to the data of Fig. 1a giving the function (Ahuja and Williams, 1991),

$$\ln[-\psi(\theta)] = a + b \ln(\theta - \theta_r) \quad [1]$$

where $\psi(\theta)$ is the soil matric potential (in kPa), θ is the volumetric soil water content, θ_r is the residual soil water content, a is the intercept, and b is the slope. Equation [1] is the inverse of the well known Brooks and Corey (1964) equation. As a result the slope b is equal to $-1/\lambda$, the inverse of the pore-size distribution index λ in Table 1.

Figure 1b is a graph of intercept a vs. slope b for all textural-class mean curves derived from data in Table 1. The regression fit to the data (solid line) has an r^2–value of 0.86, indicating a high linear relationship ($a = p + qb$). The dashed line in Fig. 1b is the fitted a vs. b relationship reported by Gregson et al. (1987) for 41 Australian and British soils. The two fitted relations from widely different soils are very close together indicating its near universality across soil classes. When each of the two fitted relations was used in scaling a new large dataset, the results were essentially the same (Fig. 3.12 and 3.13 of Williams and Ahuja, 2003). The two soils in Fig. 1b that fall off the regression line were silty loam and clay. The matric $\psi(\theta)$ and θ data for these soils were based on the analysis of 1206 and 291 soil samples respectively, and the geometric mean of these data was used in Fig. 1b. If these two soils were removed from Fig. 1b, the fitted line presented by Gregson et al. (1987) came even closer to agreeing with the trend line fitted to Rawls et al. (1982) data (not shown).

Figure 1c presents the results of scaling the textural-class mean water retention curve using the fitted a vs. b relation of the solid line in Fig. 1b. The scaled ψ in the figure is the right-hand side of

$$\ln[(\theta - \theta_r)] = \{\ln[-\psi(\theta)] - p\}b - q \quad [2]$$

where $p = -0.52$ and $q = 0.67$ (Fig. 1b). Figure 1c indicates very close scaling of the curves in Fig. 1a (Williams and Ahuja, 2003).

Figure 2 shows two new relationships with λ. Figure 2a shows the relationship between K_s and λ for the textural-class mean data in Table 1. Figure 2b shows the relationship between the bubbling pressure ($-\psi_b$) and λ. Both relationships have fairly high r^2–values (0.94 and 0.82) as represented by the following power law equations,

$$\ln K_s = 3.62(\ln \lambda) + 4.83 \quad [3]$$

$$\ln \psi_b = -1.05(\ln \lambda) + 1.43 \quad [4]$$

The two off-points in Fig. 2b are for soil, loam, and sandy clay loam. We do not know the reasons why they are off from the main trend of other soils; perhaps the methods of measurement and/or the nature of soil cores were different.

As indicated above, all the parameters of the soil water retention and hydraulic conductivity functions are implicitly

Table 2. RZWQM simulation scenarios for the 11 textural-class mean soils.

Scenario	Rainfall intensity	Duration of rain event	Initial soil water pressure head	Scenario	Wetting depth	Duration of redistribution	Initial soil water pressure head
	cm h^{-1}	h	kPa		cm	d	kPa
1	20	5	−1500	9	10	7	−1500
2	10	5	−1500	10	30	7	−1500
3	5	5	−1500	11	60	7	−1500
4	2.5	5	−1500	12	100	7	−1500
5	20	5	−100	13	10	7	−100
6	10	5	−100	14	30	7	−100
7	5	5	−100	15	60	7	−100
8	2.5	5	−100	16	100	7	−100

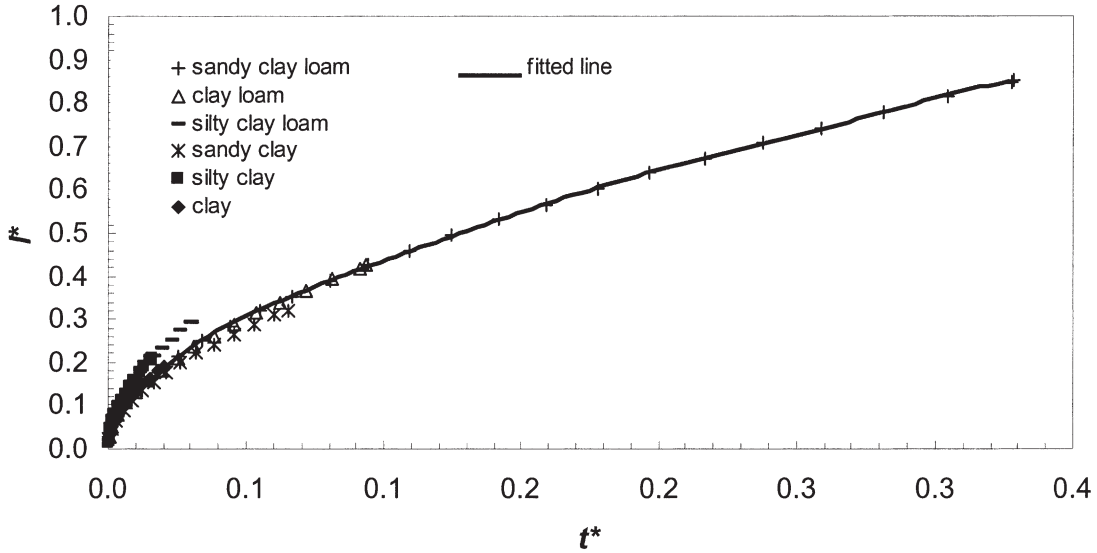

Fig. 3. Plot of the normalized cumulative infiltration (I_*) versus normalized time (t_*) for the textural mean soils that underwent near instantaneous ponding at rainfall intensities of 20 and 10 cm h^{-1} and an initial pressure head at −1500 kPa.

related to the slope λ across the 11 textural classes, assuming a constant average θ_r value for each class. Both $\psi(\theta)$ and $K(\theta)$ functions derived from these parameters turned out to be implicit and complex functions of λ.

We expect that the introduction of above hydraulic properties shown to be related to λ into the Green–Ampt equation for infiltration, subject to specified initial and boundary conditions, will give simulated infiltration that will be some function of λ and time. Similarly, the redistribution of soil water content following infiltration or an initial wetting depth will be a function of λ and time. That is, there will be a relationship among different soil types based on their λ-values for infiltration and redistribution of soil water at any given time.

Scaling Infiltration Based on Green–Ampt Model and λs

Some simple cases of infiltration from different soil types can be scaled by normalizing with respect to hydraulic conductivity, a capillary drive parameter, and soil saturation deficit (Smith, 2002, pg. 97–103), that is, using the dimensional analysis technique. For infiltration under instantaneous ponding (rainfall rate > initial infiltration rate), the cumulative infiltration I, and cumulative time t, are normalized as

$$I_* = \frac{I - K_i t}{G(\theta_s - \theta_i)} \quad [5]$$

$$t_* = \frac{t(K_s - K_i)}{G(\theta_s - \theta_i)} \quad [6]$$

where I_* and t_* are the normalized or scaled values of cumulative infiltration and time, respectively, K_i is the constant unsaturated hydraulic conductivity at the initial soil water content before the wetting event is initiated, θ_i, assumed uniform with depth, θ_s is the effective saturated water content attained during infiltration, K_s is the corresponding saturated conductivity, and G is the capillary drive or wetting-front pressure head defined as follows for a small θ_i relative to θ_s:

$$G = \frac{1}{K_s}\int_{-\infty}^{\psi_h} K(\psi)d\psi + \psi_b \quad [7a]$$

For the Brooks–Corey formulation of soil hydraulic properties and Campbell's (1974) approximation for the log–log slope of $K(\psi) = 2 + 3\lambda$, Eq. [7a] results in (Smith, 2002; pg. 71):

$$G = \frac{2 + 3\lambda}{1 + 3\lambda}\psi_b \quad [7b]$$

Since ψ_b is a function of λ (Eq. [4]), G is a function of λ alone. Except under very wet initial conditions, the K_i in Eq. [5] and [6] can be neglected giving (See Fig. 6.2 in Smith, 2002),

$$I_* = \frac{I}{G(\theta_s - \theta_i)} \quad [8]$$

$$t_* = \frac{tK_s}{G(\theta_s - \theta_i)} \quad [9]$$

For the cases examined in this study, K_i is set to zero. For an instantaneous ponding condition, the exact solution of the Green–Ampt Model of infiltration is ($K_i = 0$),

$$K_s t = I - G(\theta_s - \theta_i)\ln\left[1 + \frac{I}{G(\theta_s - \theta_i)}\right] \quad [10]$$

which scales to

$$t_* = I_* - \ln[1 + I_*] \quad [11]$$

For infiltration under constant rainfall rates, r, where ponding is not instantaneous (rainfall rate < initial infiltration rate), the

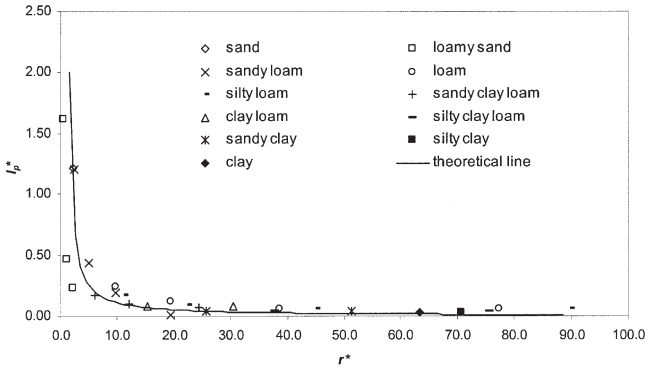

Fig. 4. Plot of the normalized cumulative infiltration at time of ponding (I_{p*}) as a function of normalized rainfall intensity (r_*) for Scenarios 1 through 4 for the 11 mean textural class soils that underwent non-instantaneous ponding at all rain intensities and an initial pressure head of −1500 kPa.

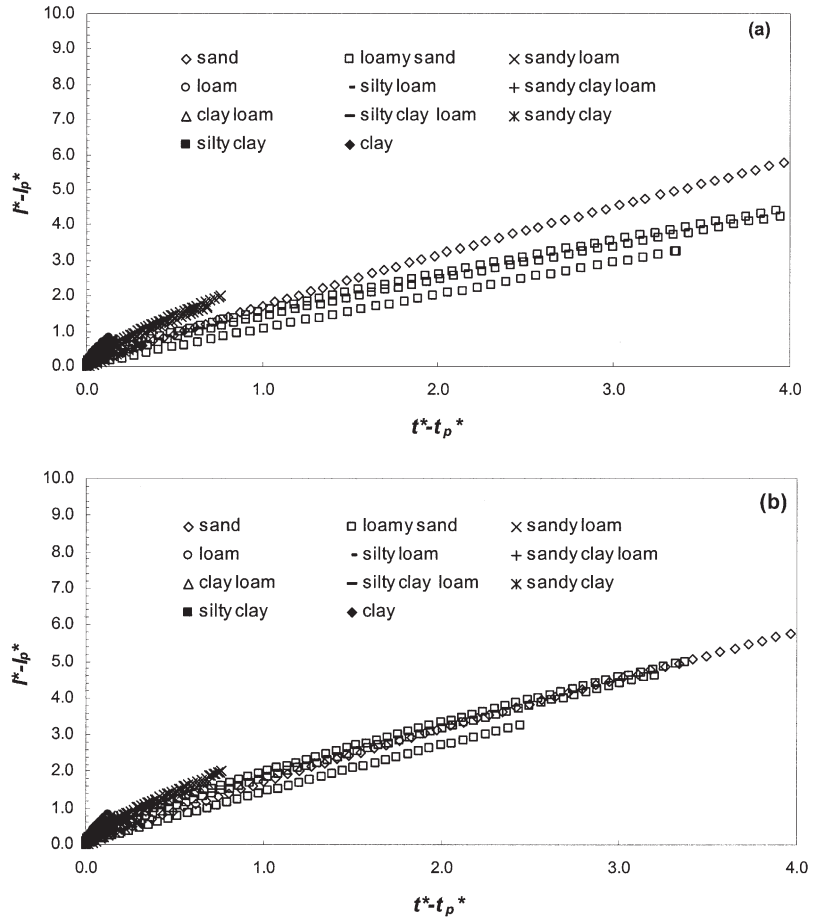

Fig. 5. (a) Plot of the normalized cumulative infiltration after ponding ($I_* - I_{p*}$) vs. normalized time after ponding ($t_* - t_{p*}$) for all four rain intensities with an initial pressure head of −1500 kPa (Scenarios 1–4) for the 11 mean textural-class soils that underwent non-instantaneous ponding; (b) Plot of the normalized ($I_* - I_{p*}$) and ($t_* - t_{p*}$) for the same data as in Fig. 5a using the RZWQM value of K_s in place of the λ-derived K_s in normalizing data for loamy sand.

cumulative infiltration until ponding, I_p for the Green–Ampt model is given as

$$I_p = \frac{K_s G(\theta_s - \theta_i)}{r - K_s} \quad [12]$$

and time to ponding, t_p, as

$$t_p = \frac{I_p}{r} = \frac{K_s G(\theta_s - \theta_i)}{r(r - K_s)} \quad [13]$$

The variables r, I_p, and t_p can be scaled as

$$r_* = \frac{r}{K_s} \quad [14]$$

$$I_{p*} = \frac{I_p}{G(\theta_s - \theta_i)} = \frac{1}{(r_* - 1)}; \quad r_* > 1 \quad [15]$$

$$t_{p*} = \frac{t_p K_s}{G(\theta_s - \theta_i)} = \frac{1}{r_*(r_* - 1)} \quad [16]$$

For the cases examined in this study, K_i, is set to zero, as relative to K_s, $K(-100$ kPa), and $K(-1500$ kPa) are negligible. Scaled cumulative infiltration after ponding for the Green–Ampt model may be expressed as ($I_* - I_{p*}$) and scaled time after ponding as ($t_* - t_{p*}$), where I_* and t_* are the scaled cumulative infiltration and time, respectively, under non-instantaneous ponding condition. If we further assume that the infiltration process after ponding begins is approximately similar to that of instantaneous ponding, a scaled solution of the Green–Ampt model for this case is:

$$(t_* - t_{p*}) = (I_* - I_{p*}) - \ln\left[\frac{1 + I_*}{1 + I_{p*}}\right] \quad [17]$$

Equation [12] for I_p can be further simplified by assuming that the gravity term is not important up to the time of ponding in all soils:

$$I_p = \frac{K_s G(\theta_s - \theta_i)}{r} \quad [18a]$$

or

$$\frac{I_p r}{\theta_s - \theta_i} = K_s G \quad [18b]$$

As one of the objectives of this study, Eq. [8] through [18] will be utilized to test the scaling of infiltration data when the normalizing variables G and K_s are derived from their λ relationships of Eq. [3], [4], and [7b].

MATERIALS AND METHODS

Eight hypothetical studies of infiltration, which encompassed four rainfall intensities and two initial profile water contents, were simulated with RZWQM (Ahuja et al., 2000) for each of 11 soil textural classes (Table 1). Upon a precipitation event in RZWQM, the method of Green and Ampt (1911)

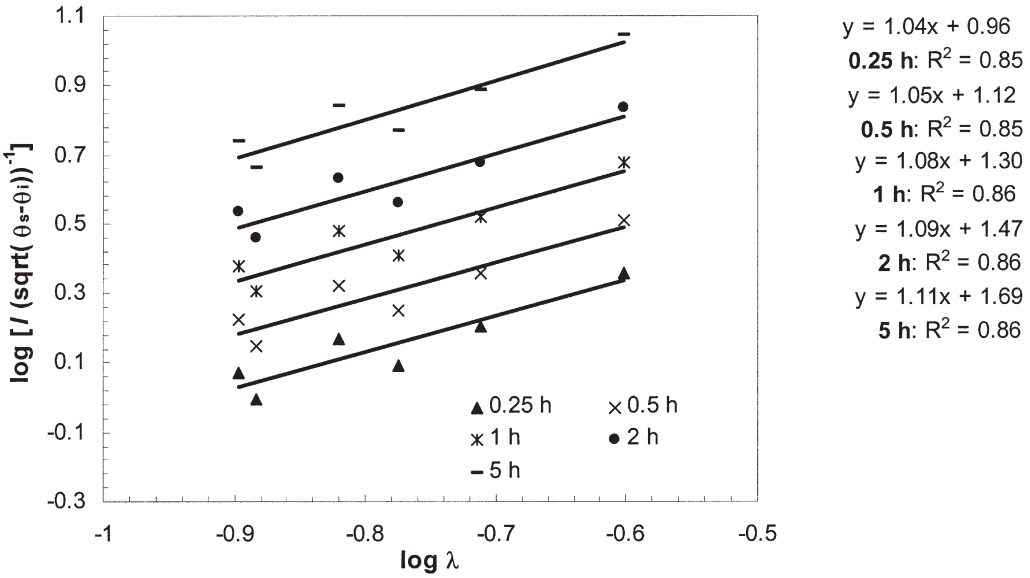

Fig. 6. Log–log relationship of $I/(\theta_s - \theta_i)^{1/2}$and the pore-size distribution index (λ) for the six finer textural-class mean soils at 20 cm h^{-1} rainfall intensity and an initial pressure head of −1500 kPa for soils that instantaneously pond.

with the wetting front pressure head obtained from the soil hydraulic conductivity curve is used to predict the infiltration rates and cumulative infiltration in the soil profile (Ahuja et al., 1993). The upper boundary condition during infiltration was the constant influx equal to the rainfall rate until the incipient ponding time, and a constant zero pressure head thereafter. Also for each textural class, eight additional simulations were performed to examine redistribution of water as a function of four wetting depths and two initial water contents at the onset of redistribution with RZWQM. The mixed form of Richards' equation for water movement in the vertical profile is used to predict the soil water profile (Johnsen et al., 1995; Ahuja et al., 2000). The upper boundary condition during redistribution was zero evaporation. The lower boundary condition in both the infiltration and redistribution study was a unit hydraulic gradient, that is, free gravity flow.

Eleven hypothetical soil columns were used in these simulation studies, one column for each of the 11 textural classes in Table 1. Each column was 3 m deep, with homogeneous hydraulic properties corresponding to the geometric mean characteristics of the associated soil textural class. The soil profiles were subjected to the initial conditions, precipitation event scenarios, and wetting depth scenarios summarized in Table 2. The 20-cm h^{-1} rainfall intensity was used as a proxy to represent ponded or flooded irrigation to attain near-instantaneous ponding in most soils; this serves as the commonly used reference case of maximum infiltration capacity. (Note: During the beginning of a rainfall event, no scenario will result in truly instantaneous ponding. There will be a short time lapse before ponding begins.)

Dimensional Analysis Methods

In *Theoretical Background and Developments*, it is shown that the Brooks–Corey parameters of soil hydraulic properties of 11 textural classes bear a strong relationship to a single parameter λ. These relationships were used to estimate K_s, ψ_b, and G from corresponding λ-values (Eq. [3], [4], and [7b]). These estimated parameters were then used to evaluate Eq. [8] through [18] for four rainfall rates of 20, 10, 5, and 2.5 cm h^{-1}, respectively, for 5 h at initial pressure heads of −1500 kPa (Scenarios 1–4 in Table 2). Depending on the soil and rainfall intensity, three outcomes can occur: (1) a soil undergoes nearly instantaneous ponding; (2) a soil undergoes non-instantaneous ponding; or (3) a soil does not pond. For soils undergoing near-instantaneous ponding, the λ-derived K_s and G parameters (Eq. [3] and [4]) and cumulative infiltration results from RZWQM simulations of the summarized scenarios were used in Eq. [8] and [9] to normalize the cumulative infiltration and time data, thereby giving I_* and t_* values. For soils undergoing non-instantaneous ponding, the simulated cumulative infiltration and time results, and the above λ-derived K_s and G values were used in Eq. [14] through [17] to provide normalized rainfall rates (r_*), normalized cumulative infiltration before ponding (I_{p*}), normalized time of ponding (t_{p*}), and an approximate scaled solution of the Green–Ampt model ($I_* - I_{p*}$). The λ-derived K_s and G estimates were used to examine the applicability of the empirically derived relationships between λ and K_s as well as between λ and ψ_b.

Regression Analysis Methods for Infiltration

The infiltration results for the scenarios summarized in Table 2 were carefully examined to identify the most suitable explicit functional relationships of infiltration with λ and time. We especially looked at the Philip's two-term equation (Philip, 1957) and Kostiakov's power law equation (Kostiakov, 1932). Based on this initial analysis, we adopted a Kostiakov-type model in which I is a product of the functions of λ and time:

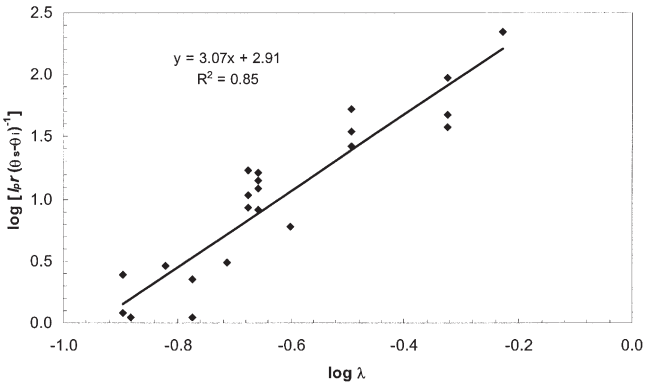

Fig. 7. Log–log plot of $I_p r/(\theta_s - \theta_i)$ as a function of λ for all rain intensities for the 11 mean textural classes.

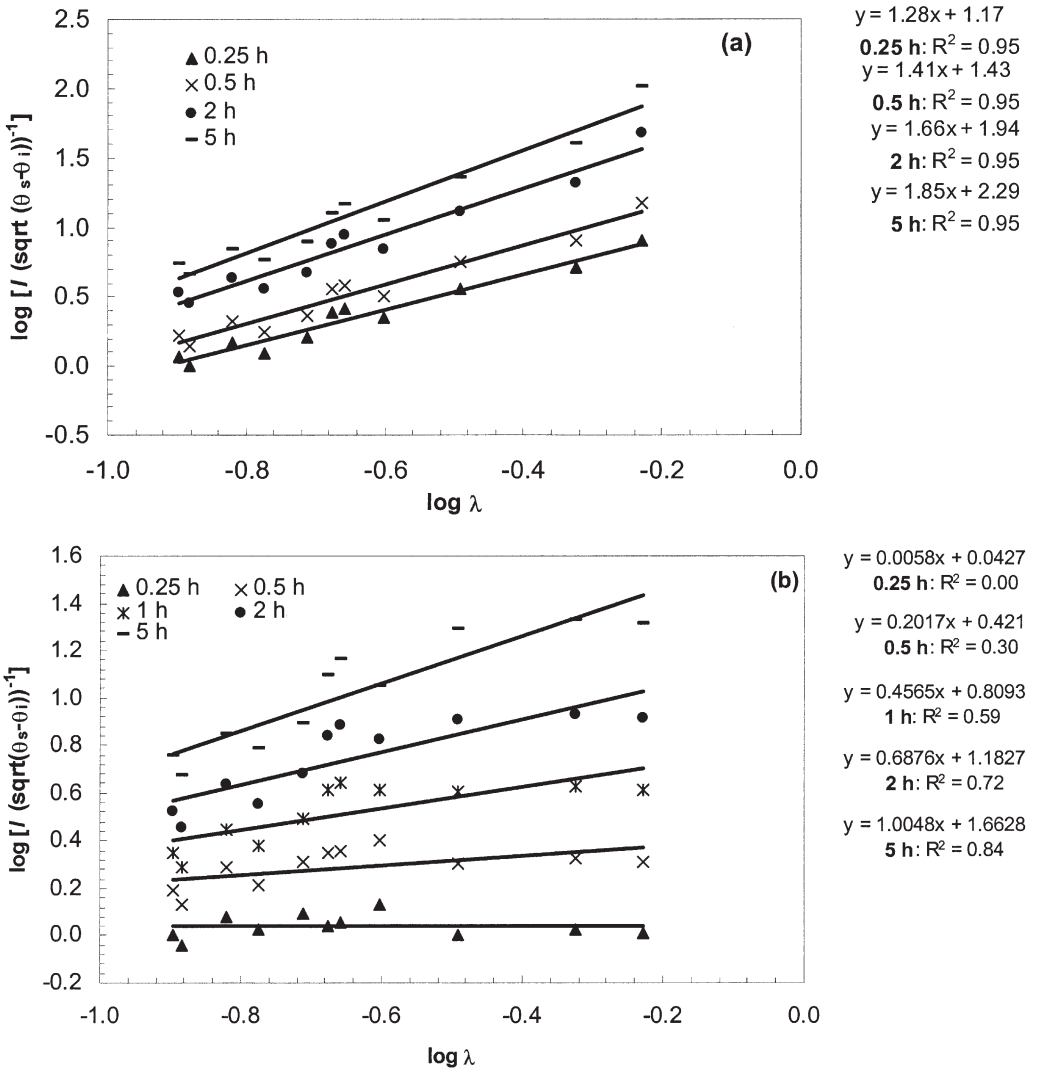

Fig. 8. (a) Log–log relationship of $I/(\theta_s - \theta_i)^{1/2}$ and the pore-size distribution index (λ) for the 11 textural-class mean soils at 20 cm h^{-1} rainfall intensity and an initial pressure head of −1500 kPa; (b) Log-log relationship of $I/(\theta_s - \theta_i)^{1/2}$ and the pore-size distribution index (λ) for the 11 textural-class mean soils at 2.5 cm h^{-1} rainfall intensity and an initial pressure head of −1500 kPa.

$$I = A(t)\lambda^B \quad [19]$$

where the exponent B may also be a mild function of time, $B = B(t)$. The λ^B term includes the effect of the soil water deficit on infiltration. In conceptual similarity to Philip's sorptivity term (S), which for the Green–Ampt model equals $[G(\theta_s - \theta_i)/2K_s]^{1/2}$, we rewrote Eq. [19] to remove the effect of $(\theta_s - \theta_i)$ term from λ^B:

$$\frac{I}{(\theta_s - \theta_i)} = \lambda^{B(t)}A(t) \quad [20a]$$

or,

$$\log\left[\frac{I}{(\theta_s - \theta_i)^{\frac{1}{2}}}\right] = B(t)\log\lambda + \log A(t) \quad [20b]$$

where $A(t)$ and B are constants for a given infiltration duration but may change with duration.

Log–log plots of $I/(\theta_s - \theta_i)^{1/2}$ versus λ for each of the 11 textural classes were made from the simulation results for rainfall durations of 0.25, 0.50, 1.0, 2.0, 3.0, 4.0, and 5.0 h for each rainfall intensity and initial condition (Table 2). A log-log linear trend line was observed in all the raw data allowing Eq. [20b] to be fitted to the simulation results for each rain intensity and duration. This approach was evaluated for its utility at characterizing cumulative infiltration for each of the several cases (near-instantaneous ponding, I, after ponding, $I - I_p$, and regardless of ponding status, I). For all 11 textural classes, the parameters $A(t)$ and $B(t)$ were determined for Scenarios 1 through 8. Within the constraints of the range of simulation, these data could be used to obtain $A(t)$ and $B(t)$ values for other rainfall intensities and durations by linear interpolation. Given these interpolated values of $A(t)$ and $B(t)$, an estimate of cumulative infiltration can be made for a soil of known λ.

Regression Analysis Methods for Redistribution

The soil water redistribution will be a function of initial wetting depth as well as the soil hydraulic properties. The λ-dependence of redistribution may also change with time much like infiltration. For each soil (i.e., each λ value) and initial depth of wetting, we fitted the average soil water content, θ^{ave}, in the redistribution profile as a function of time as follows:

Table 3. Log-log linear relationships between cumulative infiltration [$I/(\theta_s - \theta_i)^{1/2}$] and the pore-size distribution index (λ) for the 11 textural-class mean soils.

Infiltration analysis			
Rain intensity	Duration	Equations for −1500 kPa	Equations for −100 kPa
cm h^{-1}	h		
20	0.25	$0.55x + 0.60$	$1.30x + 1.19$
20	0.50	$1.14x + 1.21$	$1.43x + 1.45$
20	1.00	$1.37x + 1.55$	$1.53x + 1.69$
20	2.00	$1.58x + 1.88$	$1.67x + 1.96$
20	3.00	$1.67x + 2.04$	$1.75x + 2.11$
20	4.00	$1.74x + 2.16$	$1.81x + 2.22$
20	5.00	$1.82x + 2.27$	$1.85x + 2.31$
10	0.25	$0.95x + 0.91$	$0.74x + 0.85$
10	0.50	$1.15x + 1.23$	$0.93x + 1.17$
10	1.00	$1.32x + 1.52$	$1.13x + 1.46$
10	2.00	$1.51x + 1.83$	$1.32x + 1.77$
10	3.00	$1.61x + 1.99$	$1.42x + 1.94$
10	4.00	$1.67x + 2.12$	$1.50x + 2.06$
10	5.00	$1.76x + 2.23$	$1.57x + 2.18$
5	0.25	$0.45x + 0.50$	$0.32x + 0.48$
5	0.50	$0.71x + 0.88$	$0.57x + 0.85$
5	1.00	$0.96x + 1.24$	$0.82x + 1.20$
5	2.00	$1.19x + 1.58$	$1.04x + 1.54$
5	3.00	$1.31x + 1.77$	$1.17x + 1.73$
5	4.00	$1.37x + 1.89$	$1.25x + 1.87$
5	5.00	$1.46x + 2.01$	$1.32x + 1.97$
2.5	0.25	$0.01x + 0.04$	$-0.16x + 0.02$
2.5	0.50	$0.20x + 0.42$	$0.04x + 0.39$
2.5	1.00	$0.46x + 0.81$	$0.31x + 0.78$
2.5	2.00	$0.69x + 1.18$	$0.55x + 1.16$
2.5	3.00	$0.83x + 1.40$	$0.70x + 1.37$
2.5	4.00	$0.94x + 1.55$	$0.77x + 1.50$
2.5	5.00	$1.00x + 1.66$	$0.78x + 1.59$

$$\theta^{ave} = \theta_s C t^{-n} \quad \text{or} \quad \log \frac{\theta^{ave}}{\theta_s} = -n \log t + \log C \qquad [21]$$

where C and n are functions of λ and initial depth of wetting, and θ^{ave} is defined as,

$$\theta^{ave} = \frac{\sum_{k}^{N} \theta_k z_k}{WD} \qquad [22]$$

Here, k is the soil layer (unitless), N is the number of soil layers (unitless), θ_k is the soil moisture content of the layer ($L^3\ L^{-3}$), z_k is the layer depth (L), and WD is the depth of the wetting front (L).

Log–log plots of θ^{ave}/θ_s versus t for the mean homogeneous soils of the 11 textural classes were made for Scenarios 9 through 16. Again, a log–log linear trend was observed in all the raw data for each soil (λ) allowing Eq. [21] to be fitted to the simulation results for each wetting depth and time after the beginning of redistribution. The parameters C and n were determined for Scenarios 9 through 16 and were plotted with respect to λ. An estimate of θ^{ave} can be made with these parameters for a soil of known λ by interpolation.

RESULTS AND DISCUSSION

λ-Scaled Cumulative Infiltration

For rainfall intensities of 20 and 10 cm h^{-1} (Scenarios 1 and 2, Table 2), some soils underwent nearly instantaneous ponding. Plots of normalized cumulative infiltration I^* as a function of normalized time t^* for the ponded soils tend to converge toward a single curve for both rainfall intensities (Fig. 3). Deviations from exact coalescence may be due to some errors in the λ-based estimations of K_s (Eq. [3]), ψ_b (Eq. [4]), and G (Eq. [7b]), small errors in RZWQM's numeric solution of the Green–Ampt equation, and the fact that the soils plotted do not exactly undergo instantaneous ponding in model simulation. Overall, the λ-based K_s and G values used in Eq. [8] through [9] normalized cumulative infiltration and time rather well. It is also noteworthy that the normalized cumulative infiltration and time results come together along a common function for both rainfall intensities of 20 and 10 cm h^{-1}, as expected.

Table 4. Log-log relationships between n and the pore-size distribution index (λ) and C and λ for the 11 textural-class mean soils at −100 kPa.

Redistribution analysis		
Wetting depth	n equations	C equations
10	$-0.14x - 0.15$	$-0.40x^2 - 1.04x + 0.35$
30	$-0.17x - 0.18$	$-0.67x^2 - 1.12x + 0.53$
60	$-0.18x - 0.17$	$-0.87x^2 - 1.28x + 0.55$
100	$-0.19x - 0.18$	$-1.03x^2 - 1.40x + 0.57$

For the non-instantaneous ponding cases, a plot of normalized infiltration at ponding time I_{p*} versus normalized rainfall intensity r_* tend to converge along a single theoretical curve for all soils and all rainfall intensities (Eq. [15], Fig. 4). Additionally, the normalized cumulative infiltration after ponding ($I_* - I_{p*}$) vs. normalized time after ponding ($t_* - t_{p*}$) for all 11 soils for Scenarios 1 through 4 tend to come together along a central curve (Fig. 5a). (Note: Due to the large number of data, it is difficult to see the data for individual soils in Fig. 5a.) In a plot of ($t - t_p$) versus ($I - I_p$) (not shown), at ($t - t_p$) = 3 h, there was a 30 times difference between the extreme ($I - I_p$) values. Comparatively, in Fig. 5a at ($t_* - t_{p*}$), there is 1.5 times difference between the extreme ($I_* - I_{p*}$) values. Therefore, a high degree of convergence was achieved in this procedure.

Deviations off the normalized curves in Fig. 4 and 5a may be due to errors in the estimation of K_s and G from λ and numerical approximation error for I_* vs. t_*. Additionally, the deviations in the curves of Fig. 5a may also be due to the approximate nature of Eq. [17]. The curve for loamy sand showed the most deviation off the converged curves in both Fig. 4 and 5a, and this was traced to underestimation of K_s derived from λ (Eq. [3]) compared with the actual K_s for this soil used in the RZWQM simulations (Table 1). If the simulation value of K_s for loamy sand was used for normalization, the ($I_* - I_{p*}$) and ($t_* - t_{p*}$) values coalesce closer on the fitted line, and further improve the relationships shown in Fig. 4 (data not shown) and 5a (see Fig. 5b).

Based on the normalization results, estimates of a soil's cumulative infiltration before and after ponding can be made if infiltration values are known for a single reference soil. For example, if the λ-value for a reference soil (ref) and for a "test" soil (j) are known, estimates of K_s, ψ_b, and G can be made through the application of Eq. [3], [4], and [7b], respectively. Further, if the reference and test soils undergo near-instantaneous ponding and the initial conditions of both soils, that is, θ_s and θ_i are known, the cumulative infiltration of the reference soil, I^{ref}, at time t can be applied to Eq. [8] to give I_*.

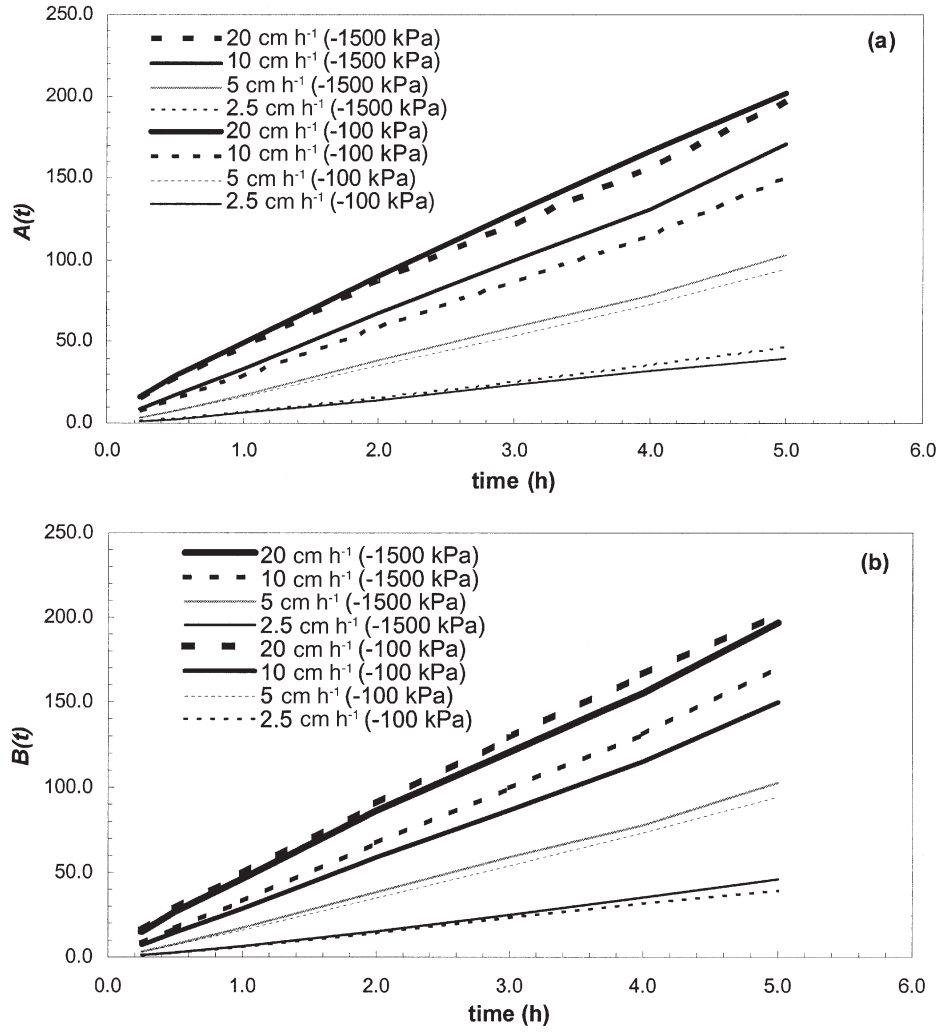

Fig. 9. (a) Variation of coefficient $A(t)$ of Eq. [20] from fitted $I_p/(\theta_s - \theta_i)^{1/2}$ vs. λ relations with infiltration times for different rainfall intensities; (b) Variation of coefficient $B(t)$ of Eq. [20] from fitted $I_p/(\theta_s - \theta_i)^{1/2}$ vs. λ relations with infiltration times for different rainfall intensities.

The normalized infiltration value, I_*, can then be used with respect to the test soil to determine that soil's cumulative infiltration by applying Eq. [8] and using the test soil's specific parameters:

$$I^j = G^j(\theta_s^j - \theta_i^j)I_* \quad [23]$$

This same methodology can be used if both soils undergo non-instantaneous ponding. The respective parameters of the reference soil mentioned above can be applied to Eq. [15] through [17] given that the time to ponding, t_p, cumulative infiltration until ponding, I_p, and cumulative infiltration, I, are known for the reference soil. Given the normalized cumulative infiltration before ponding, I_{p*}, Eq. [15] and [16] can be used to determine I_p^j and t_p^j for the test soil. Likewise, the normalized cumulative infiltration after ponding, $I_* - I_{p*}$, for a reference soil can be applied to determine cumulative infiltration after ponding, $I^j - I_p^j$, for the test soil using Eq. [17].

λ-Based Explicit Relationships for Cumulative Infiltration

Plotting log $I/(\theta_s - \theta_i)^{1/2}$ as a function of log λ (Eq. [20]) for the 20 cm h^{-1} rainfall intensity Scenario 1) showed there is a strong relationship between I and λ for all rainfall durations for the soils that underwent instantaneous ponding as indicated by the high r^2–values (0.85–0.86) (Fig. 6). (To make Fig. 6 easier to read, only selected times were plotted). The parallel nature of the curves for each time of interest is interesting, as it would allow scaling between the different times. For soils that underwent non-instantaneous ponding in Scenarios 1 through 4, a log–log plot of $I_p r/(\theta_s - \theta_i)$ versus λ (Eq. [18]) for all rain intensities is shown in Fig. 7. A linear trend line was fitted through the data giving a relatively high r^2–value of 0.85. However, when Eq. [20] was applied to data for $(I - I_p)$, that is, $(I - I_p)/(\theta_s - \theta_i)^{1/2}$, for non-instantaneous ponding cases, the relationships varied with rain intensity as expected; high r^2–values were observed for the 20-cm h^{-1} rain intensity (Scenario 1) except for $t = 0.25$ h, but no strong relationship was observed for the 2.5 cm h^{-1} intensity (Scenario 4). At smaller times and lower intensities, the $(I - I_p)$ differences among soils are small as the rain infiltrates in all soils; hence, $(I - I_p)$ is a poor function of λ.

The best relationships were observed when cumulative infiltration, $I/(\theta_s - \theta_i)^{1/2}$, regardless of ponding status

was plotted against λ; a log–log plots of $I/(\theta_s - \theta_i)^{1/2}$ versus λ for different times are shown in Fig. 8a and 8b for the two extreme intensities, 20 and 2.5 cm h^{-1}. (To make Fig. 8a and 8b easier to read, only selected times were plotted). Note that the relationship between $I/(\theta_s - \theta_i)^{1/2}$ and λ is better at higher rainfall intensities and longer durations. Except for the case of the lowest intensity of 2.5 cm h^{-1} and shorter durations (≤1 h), the r^2–values are 0.72 to 0.95. As expected, for the 2.5 cm h^{-1} intensity and short rainfall durations, the r^2–values are relatively lower due to the fact that initially all the rainfall infiltrates into the soils regardless of the λ-value, thus resulting in little if any relationship between cumulative infiltration and λ. Similar trends of r^2–values were observed with respect to Scenarios 5 through 8 as well. Table 3 summarizes the fitted equations for the different infiltration experiments (Scenarios 1–8, Table 2) over the course of time.

The functions $A(t)$ and $B(t)$ of Eq. [20] are shown in Fig. 9a and 9b, respectively. These functions were estimated from the fitted regression lines for all the log–log plots of $I/(\theta_s - \theta_i)^{1/2}$ and λ and the different rainfall durations, intensities and initial pressure heads. The results show that $A(t)$ and $B(t)$, and hence, the depth of infiltration are a function of λ and time, as expected, as well as that of the rainfall intensity, and to a smaller degree, initial soil water content. Given the rainfall rate and soil type, the coefficients can be interpolated from Fig. 9a and 9b to provide a rough estimate of cumulative infiltration for that soil by applying the estimated $A(t)$ and $B(t)$ values to Eq. [20].

Additionally, for somewhat uncertain field conditions, if the cumulative infiltration for different infiltration times is known for a reference soil, the estimates from Eq. [20] can be compared with the measured values. Based on the difference between the estimated and measured values for the reference soil: (1) the coefficients [$A(t)$] for Eq. [20b] could be adjusted while keeping $B(t)$ the same to predict cumulative infiltration for other soils; or (2) the estimations for other soils may be increased or decreased relative to the difference observed with respect to the reference soil.

λ-Based Explicit Relationships for Redistribution

Log–log plots of θ^{ave}/θ_s versus t (Eq. [21]) for different redistribution times, following four initial wetting depths and an initial pressure head of −1500 kPa, are shown in Fig. 10 for two extreme soils, sand and clay, respectively. High r^2–values were observed for sand, clay, and every other soil for Scenarios 9 through 16. The r^2–values increased with shallower initial wetting depth. Semi-log plots of n vs. λ and C vs. λ are shown in Fig. 11 for Scenarios 9 through 12. The observed dependence between λ and both C and n indicates a strong relationship between λ and θ^{ave}. For clayey soils (small λ values), the absolute values of n are larger for shallower initial depths of wetting than for deeper depths; whereas for sandy soils (large λ values) the n values for different initial wetting depths are similar. The reverse trend is observed with respect to C values. The n vs. λ and C vs. λ relations for the initial pressure head of −100 kPa (Scenarios 13–16, Table 2) were only slightly different from those for −1500 kPa, with similar r^2–values; the fitted equations for Scenarios 13 through 16 are summarized in Table 4.

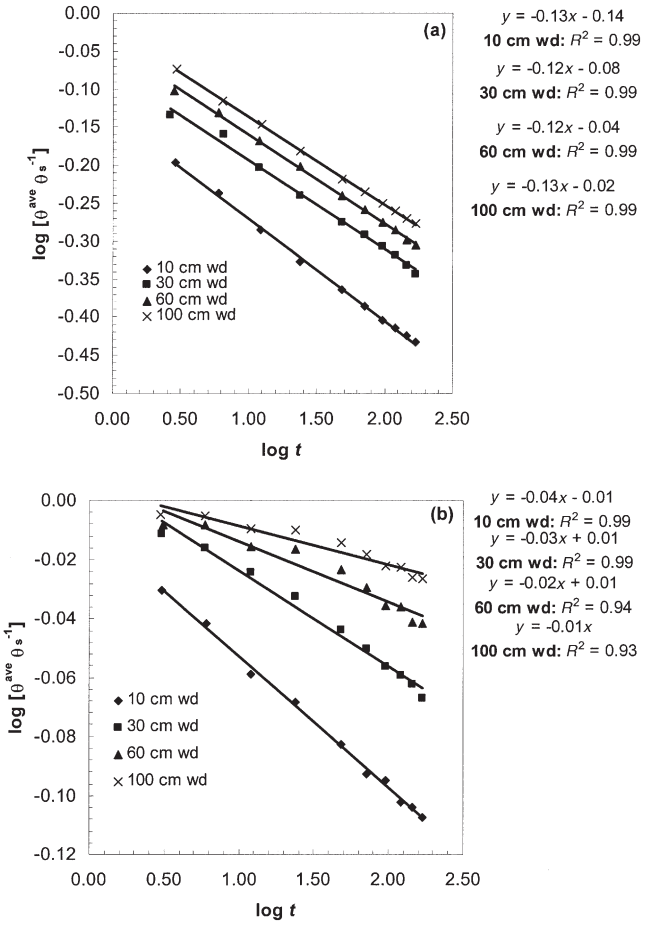

Fig. 10. (a) Log–log relationship of θ^{ave}/θ_s and time for sand for four initial wetting depths and an initial pressure head of −1500 kPa; and (b) Log-log relationship of θ^{ave}/θ_s and time for clay for four initial wetting depths and an initial pressure head of −1500 kPa.

Because trend lines fitted through the data have high r^2–values, one can interpolate n and C for other soils and initial wetting depths. These estimated coefficients can be applied to Eq. [21] to determine θ^{ave} for a given redistribution time.

CONCLUSIONS

From the *Theoretical Background and Developments* section, it is indicated that all the parameters of the soil water retention and hydraulic conductivity functions are implicitly related to the slope λ across the 11 textural classes, assuming a constant average θ_r value for each class. The λ-dependence is shown here to also extend to infiltration and soil water storage relations across the soil classes. For the 11 mean textural class soils considered in this study, the cumulative infiltration results from four rainfall intensities and two initial pressure heads simulated by using the complete hydraulic properties of each

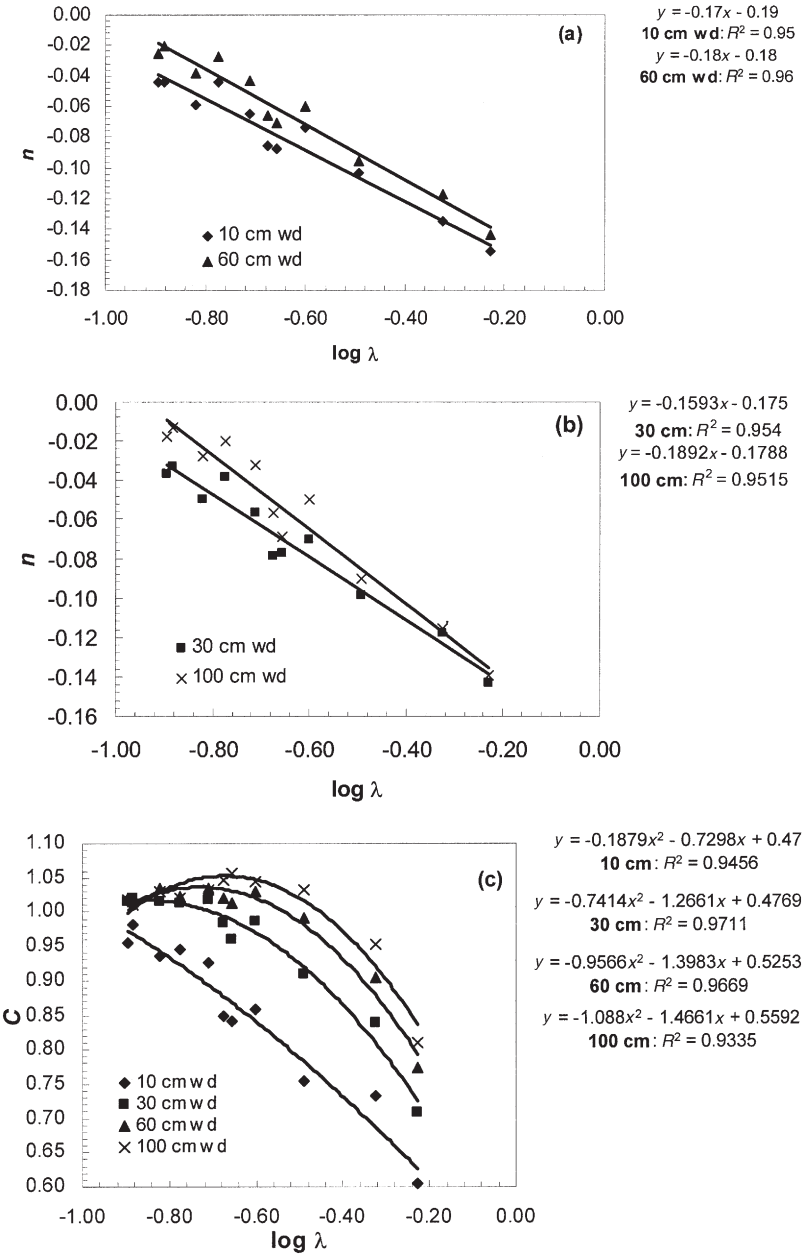

Fig. 11. (a) Variation of coefficient *n* of Eq. [21] for the 10- and 60-cm wetting depths and an initial pressure head of −1500 kPa; (b) Variation of coefficient *n* of Eq. [21] for the 30- and 100-cm wetting depths and an initial pressure head of −1500 kPa; and (c) Variation of coefficient *C* of Eq. [21] for four initial depths and an initial pressure head of −1500 kPa.

soil are shown to be scaled through λ-derived normalizing variables based on the Green–Ampt infiltration model. For the near instantaneous ponding conditions, it was observed that the plots of normalized cumulative infiltration, I_*, and time, t_*, coalesced together reasonably well, regardless of rainfall intensity. Similarly, for non-instantaneous ponding conditions, it was observed that the plots of normalized cumulative infiltration until ponding time, I_{p*}, and normalized rainfall rate, r_*, as well as those of $(I_* - I_{p*})$ and $(t_* - t_{p*})$ followed the same trend as all 11 soils, converged to a normalized curve. The convergence was observed regardless of rainfall intensity. These results indicate λ-based scaling relationships across soil textural classes and allow estimation of infiltration into unknown soils of known λs from infiltration data for a reference soil for different rain intensities and initial conditions.

Cumulative infiltration, I, from several rainfall intensities, and the average water content of the wetted profile, θ^{ave}, during soil water redistribution from several initial wetting depths in a soil system, also had direct relationships to the pore-size distribution index, λ, for the 11 soil textural classes. The coefficients of determination (r^2) for log $I/(\theta_s - \theta_i)^{1/2}$ versus log λ were very high for high rainfall intensities and long durations. For low rainfall intensities and shorter durations, the r^2–values were lower, as all the rain infiltrated in most soils irrespective of their λ-values. For these cases, cumulative infiltration before ponding was highly correlated with the λ-values. The r^2–values for log θ^{ave}/θ_s versus log

t were very high. Fitted curves to these log θ^{ave}/θ_s versus log *t* plots provided the empirical coefficients, *n* and *C*. These empirical coefficients had strong curvilinear relationships with λ. These empirically fitted relationships can serve as nomographs to estimate *I* and θ^{ave} for any soil of known λ and any rain intensity and duration by interpolations between the given conditions. Estimates can be calculated directly from the regression line and respective empirical coefficients for a soil. This method can also be used for quick estimation of hydraulic properties.

The above results enhance our understanding of the relationships among soil types for infiltration and soil water contents under different boundary conditions and enhance our ability to quantify and manage spatial variability. However, these results are for idealized situations. Under natural field conditions, soil layering and patterns of rainfall are much more complex. Further research is needed to explore extension of the relationships developed here to these conditions. For layered soils, it may be assumed that the λ of the topsoil controls the infiltration process in most cases. For redistribution it may be the harmonic mean λ of the profile. It is hoped that we can build on these simple and generally encouraging results, to meet the critical needs of: (i) estimating the spatial variability of soil water over large areas for site-specific management; and (ii) for scaling up results in modeling from plots to fields to watersheds.

REFERENCES

Ahuja, L.R., J.W. Naney, R.E. Green, and D.R. Nielsen. 1984. Macroporosity to characterize spatial variability of hydraulic conductivity and effects of land management. Soil Sci. Soc. Am. J. 48:699–702.

Ahuja, L.R., J.W. Naney, and R.D. Williams. 1985. Estimating soil water characteristics from simpler properties or limited data. Soil Sci. Soc. Am. J. 49:1100–1105.

Ahuja, L.R., and R.D. Williams. 1991. Scaling water characteristic and hydraulic conductivity based on Gregson-Hector-McGowan approach. Soil Sci. Soc. Am. J. 55:308–319.

Ahuja, L.R., Decoursey, D.G., Barnes, B.B., and Rojas, K.W. 1993. Characteristics of macropore transport studied with the ARS root zone water quality model. Trans. ASAE. 36:369–380.

Ahuja, L.R., K.W. Rojas, J.D. Hanson, M.J. Shaffer, and L. Ma. 2000. Root Zone Water Quality Model: Modeling management effects on water quality and crop production. Water Resources Publications, LLC, Highlands Ranch, CO.

Brooks, R.H., and A.T. Corey. 1964. Hydraulic properties of porous media. Hydrological Paper no. 3. Colorado State University, Fort Collins.

Campbell, G.S. 1974. A simple method for determining unsaturated conductivity from moisture retention data. Soil Sci. 117:311–314.

Green, R.E., L.R. Ahuja, S.K. Chong, and L.S. Lau. 1982. Water conduction in Hawaii oxic sols. Technol. Rep. 143. Water Resources Research Center. University of Hawaii, Honolulu.

Green, W.H., and G.A. Ampt. 1911. Studies of soil physics, 1. Flow of air and water through soils. J. Agric. Sci. 4:1–24.

Gregson, K., D.J. Hector, and M. McGowan. 1987. A one-parameter model for the soil water characteristic. J. Soil Sci. 38:483–486.

Hunt, A.G., and G.W. Gee. 2002a. Water-retention of fractal soil models using continuum percolation theory. Vadose Zone J. 1:252–260.

Hunt, A.G., and G.W. Gee. 2002b. Application of critical analysis to fractal porous media: Comparison with examples from the Hanford site. Adv. Water Resour. 25:129–146.

Johnsen, K.E., Liu, H.H., Dane, J.H., Ahuja, L.R., and Workman, S.R. 1995. Simulating fluctuating water tables and tile drainage with a modified root zone water quality model and a new model WAFLOWM. Trans. ASAE. 38: 75–83.

Kostiakov, A.N. 1932. On the dynamics of the coefficient of water-percolation in soils and on the necessity of studying it from a dynamic point of view for purposes of amelioration. Trans. 6th Comm. ISSS, Russian Part A:17–21.

Miller, E.E., and R.D. Miller. 1956. Physical theory for capillary flow phenomena. J. Appl. Phys. 27:324–332.

Nielsen, D.R., J.W. Hopmans, and K. Reichardt. 1998. An Emerging technology for scaling field soil-water behavior in Scale Dependence and Scale Invariance in Hydrology, Cambridge University Press, Cambridge, UK.

Pachepsky, Y., D.E. Radcliffe, and H.M. Selim. (ed.) 2003. Scaling methods in soil physics. CRC Press, Boca Raton, FL.

Peck, A.J., R.J. Luxmoore, and J.L. Stolzy. 1977. Effect of spatial variability of soil hydraulic properties in water budget modeling. Water Resour. Res. 13:348–353.

Philip, J.R. 1957. Theory of infiltration 1. The infiltration equation and it's solution. Soil Sci. 83:345–358.

Rawls, W.J., Brakensiek, D.L., and Saxton, K.E. 1982. Estimation of soil water properties. Trans. ASAE. 25:1315–1320.

Rieu, M., and G. Sposito. 1991. Fractal fragmentation, soil porosity, and soil water properties. I. Theory. Soil Sci. Soc. Am. J. 55:1231–1238.

Russo, D., and E. Bresler. 1980. Scaling soil hydraulic properties of a heterogeneous field. Soil Sci. Soc. Am. J. 44:681–683.

Sharma, M.L., and R.J. Luxmoore. 1979. Soil spatial variability and its consequences on simulated water balance. Water Resour. Res. 15:1567–1573.

Sharma, M.L., G.A. Gander, and C.G. Hunt. 1980. Spatial variability of infiltration in a watershed. J. Hydrol. (Amsterdam) 45:101–122.

Simmons, C.S., Nielsen, D.R., and Biggar, J.W. 1979. Scaling of field-measured soil water properties. Hilgardia. 47: 77–154.

Smith. Roger E. 2002. Infiltrability models: Comparisons and application. p. 97–118. *In* K.R.J. Smettem et al. (ed.) Infiltration theory for hydrologic applications. American Geophysical Union, Washington, DC.

Tillotson, P.M., and D.R. Nielsen. 1984. Scale factors in soil science. Soil Sci. Soc. Am. J. 48:953–959.

Tyler, S.W. and Wheatcraft, S.W. 1990. Fractal processes in soil water retention. Water Resour. Res. 26:1047–1054.

Warrick, A.W., G.M. Mullen, and D.R. Nielsen. 1977. Scaling field-measured soil hydraulic properties using a similar-media concept. Water Resour. Res. 13:355–362.

Warrick, A.W., and A. Amoozegar-Fard. 1979. Infiltration and drainage calculations using spatially scaled hydraulic properties. Water Resour. Res. 15:1116–1120.

Williams, R.D., and L.R. Ahuja. 1991. Estimating soil water characteristics using physical properties and limited data. p.405. *In* M.Th. van Genuchten (ed.) Indirect methods for estimating the hydraulic properties of unsaturated soils. Proc. Int. Works. Riverside, CA. 11–14 Oct. 1989. Univ. of Calif. Press. Riverside.

Williams, R.D., and R.D. Ahuja. 2003. Scaling and estimating the soil water characteristic using a one-parameter model. p. 35–48. *In* Scaling methods in soil physics. CRC Press, London.